Journal of Fluids and Structures (1998) **12,** 57–83

LOW-GRAVITY PROPELLANT SLOSH ANALYSIS USING SPHERICAL COORDINATES

M. UTSUMI

Machine Element Department, Research Institute, Ishikawajima-Harima Heavy Industries Company Ltd.
3-1-15 Toyosu, Koto-ku, Tokyo 135, Japan

(Received 3 October 1996 and in revised form 2 October 1997)

Low-gravity sloshing in a convex axisymmetrical container subjected to lateral excitation is formulated by a variational principle and is solved analytically by a modal analysis method. The use of spherical coordinates enables us: (i) to determine analytically the system of characteristic functions for an arbitrary convex container, for which time-consuming and expensive numerical methods have been used in the past; (ii) to express the liquid surface and its dynamical displacement in the form of a single-valued function even when the liquid surface curves strongly, due to surface tension; and (iii) to satisfy the compatibility condition for the liquid surface displacement at the container wall. The variational principle is transformed into a frequency equation in the form of a standard eigenvalue problem by the Galerkin method, in which admissible functions for the velocity potential and the liquid surface displacement are determined analytically in terms of the Gauss hypergeometric series. Since this process is analytical and the dimension of the eigenvalue problem for obtaining a sufficiently converged solution is very low, little computation time and cost are involved. Numerical results show that: (a) the influences of the Bond number on the eigenfrequency are different for high and low liquid-filling levels; (b) neglecting the surface tension underestimates the magnitude of the surface oscillation; and (c) the liquid depth yielding the maximum slosh force and moment increases with decreasing Bond number.

1. INTRODUCTION

ASSOCIATED WITH THE DYNAMICS AND CONTROL ANALYSIS of a space vehicle, propellant sloshing, i.e. the oscillatory motion of a liquid propellant in a moving container, is a subject of great importance (Abramson 1966). Sloshing has an unfavourable influence on vehicle stability and may disturb the flight trajectory or cause high stresses on the structural-supporting systems of the vehicle. Especially for large vehicles, the propellant contributes a non-negligible portion to the total mass of the vehicle, so that the importance of sloshing is accentuated, and it is essential to examine and understand the slosh dynamics in the low-gravity space environment.

In the low-gravity sloshing problem, the surface tension of the liquid plays an overwhelming role in comparison to the gravitational force as the restoring force governing the oscillatory motion of the liquid surface. Due to the surface tension effect, the liquid surface can be curved strongly even in the undisturbed static case. This static liquid surface is called the meniscus. The strongly curved meniscus makes the problem geometrically more complicated than the sloshing problem under normal gravity, especially for an arbitrary axisymmetrical container with curved walls and top. As a preliminary step to the dynamical

0889–9746/98/010057 + 27 $25.00/fl970125

slosh analysis, we must therefore determine the geometry of the meniscus by solving a nonlinear differential equation iteratively (Utsumi 1989).

Studies on low-gravity sloshing have been conducted for a cylindrical container (Satterlee & Reynolds 1964; Dodge & Garza 1967; Tong 1967; Bauer & Siekmann 1971; Peterson *et al.* 1989) and for an arbitrary axisymmetrical container (Yeh 1967; Concus *et al.* 1969; Chu 1970; Dodge & Garza 1970; Dodge *et al.* 1991; Hung & Lee 1992). For an arbitrary axisymmetrical container, these previous studies did not develop any analytical expressions for the characteristic functions constituting the modal functions of the velocity potential and the liquid surface displacement. Numerical procedures were applied instead, and the computation time and cost increased dramatically when the computational mesh was refined. Therefore, in order to solve this problem and further enhance the study on sloshing, this paper develops a new analytical method for determining the characteristic functions for an arbitrary axisymmetrical container.

In previous studies (Utsumi 1988, 1989), an analytical method was presented for determining the characteristic functions by using spherical coordinates whose origin is at the top of the cone that is tangent to the container at the contact line of the meniscus with the container wall. This analytical method requires little computation time and cost and, furthermore, has the following merits over numerical methods: (i) the mathematical formulation allows the liquid surface and its dynamical displacement to be expressed as a single-valued function, even when the liquid surface curves strongly due to the surface tension in a low-gravity space environment; (ii) the kinematic compatibility condition for the liquid surface displacement can be satisfied at the container wall by considering only one component of the liquid surface displacement vector. The method is thus a geometrically convenient solution of the low-gravity sloshing problem for an arbitrary axisymmetrical convex container.

In the previous papers (Utsumi 1988, 1989), the meniscus shape and the eigenfrequency were determined for a prescribed liquid-filling level. The purpose of the present paper is to deal with a more advanced and practically important problem, i.e. predicting the responses of surface slosh motion and slosh force and moment to lateral excitation of the container. Furthermore, additional discussion is presented on numerical results for the eigenfrequency.

2. FORMULATION OF THE PROBLEM

2.1. Computational Model

The geometry is defined as in Figure 1, where an ellipsoidal container is drawn as typical example for an axisymmetrical container. The container is subjected to the lateral acceleration $\ddot{f}(t)$ in the x-direction. The low-g sloshing is characterized by the strongly curved meniscus M, which is a plane surface in normal gravity. It is assumed that the liquid motion is inviscid, incompressible and irrotational, and the container is rigid.

In this paper, the meniscus shape $R_M(\theta)$ is considered to be known, since it has been calculated in a previous study (Utsumi 1989). Moreover, the oscillatory displacement of the liquid surface ζ from its equilibrium position M is assumed to be small within the framework of linear theory.

2.2. Spherical Coordinate System

As shown in Figure 1, a spherical coordinate system (R, θ, φ) is introduced and the liquid surface displacement ζ is considered in the R-direction. The origin O is chosen as the apex of

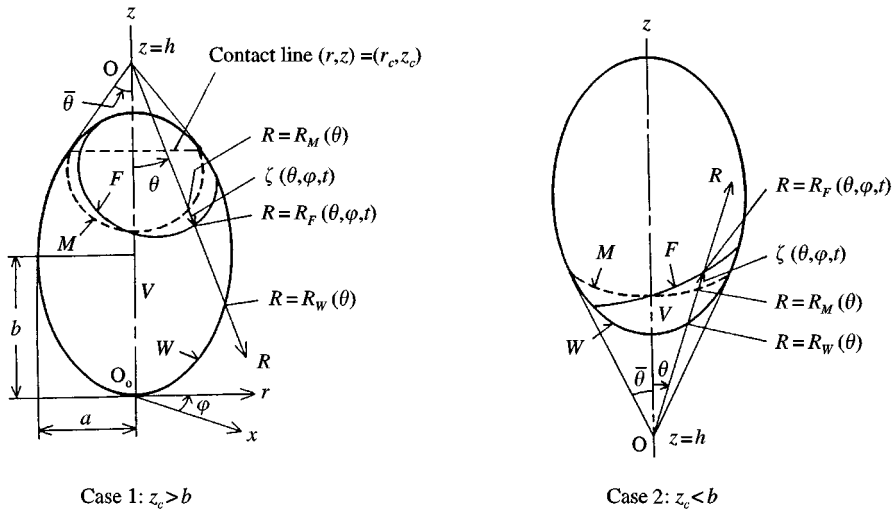

Figure 1. Axisymmetrical container and coordinate systems (z_c denotes the z-coordinate of the contact line of the meniscus M with the container wall W),

the cone whose side wall is tangent to the container wall at the contact line of the meniscus with the container wall. By using the spherical coordinate system, the meniscus M, the disturbed liquid surface F, and the container wall W can be expressed as

$$M\colon\ R = R_M(\theta), \tag{1}$$

$$F\colon R = R_F(\theta, \varphi, t) = R_M(\theta) + \zeta(\theta, \varphi, t), \tag{2}$$

$$W\colon R = R_W(\theta). \tag{3}$$

Using the spherical coordinate system has the following three merits.

(i) The functions R_M, R_F and ζ can be expressed as single-valued functions with respect to θ and φ. This is convenient for the mathematical formulation. If one uses cylindrical coordinates [e.g. Yeh (1967)], the z-coordinates of the meniscus and liquid surface elevation are two-valued functions with respect to r and φ for high liquid-filling levels (see Case 1 in Figure 1) due to the very small contact angle between the liquid surface and the container wall (Neu & Good 1963).

(ii) The liquid surface displacement at the wall can be made tangential to the container wall. Namely, the surface displacement does not penetrate nor detach from the container wall, so the compatibility condition required for the surface displacement at the container wall can be satisfied. Note that only one component of the surface displacement vector needs to be considered for satisfaction of the compatibility condition.

(iii) An analytical method can be applied to derive the characteristic function for an arbitrary axisymmetrical container, as explained in detail in Section 3.1.

As shown in Figure 1, the position of the origin O of the spherical coordinate system introduced here depends on the liquid-filling level z_c. The origin is above the container for $z_c > b$ (Case 1) and below otherwise (Case 2). The maximum angle $\bar{\theta}$ is given by

$$\bar{\theta} = \tan^{-1}(r_c | z_c - h|), \tag{4}$$

where h is the z-coordinate of the origin O, which is determined by the container geometry. The relation between (r, z) and (R, θ) is

$$r = R\sin\theta, \quad z = h - \varepsilon R\cos\theta, \tag{5}$$

where ε is defined as

$$\varepsilon = 1 \ (\text{for } z_c > b), \quad \varepsilon = -1 \ (\text{for } z_c < b) \tag{6}$$

which is convenient for simultaneous mathematical description of Cases 1 and 2 (Figure 1).

2.3. The Variational Principle

For the present problem, the variational principle can be written in the form

$$\delta \int_{t_1}^{t_2} \left\{ \iiint_V (p_l - p_g)\,\mathrm{d}V - \iint_F \sigma\,\mathrm{d}F \right\} \mathrm{d}t = 0, \tag{7}$$

where the Lagrangian within braces can be derived as follows. When neglecting surface tension and gas pressure, the Lagrangian density equals the liquid pressure (Seliger & Whitham 1968), so that the Lagrangian becomes equal to $\iiint_V p_l\,\mathrm{d}V$. From this we must subtract the potential energy due to the gas pressure $p_g V$ and that due to the surface tension $\iint_F \sigma\,\mathrm{d}F$ in order to estimate the Lagrangian for the case under consideration here. The gas pressure is assumed to be constant, since the gas density is much smaller than the liquid density.

From the pressure equation for unsteady flow, p_l can be expressed in terms of the velocity potential Φ,

$$p_l = p_0 - \rho_f \left\{ \frac{\partial \Phi}{\partial t} + g(z - z_0) + \frac{1}{2}(\nabla\Phi)^2 + \dot{G}_0(t) \right\}, \tag{8}$$

where $G_0(t)$ is an arbitrary time-dependent function.

Equation (8) is written in space-fixed coordinates X, Y and Z. It may be rewritten in tank-fixed coordinates x, y and z by using the relations

$$x = X - f(t), \quad y = Y, \quad z = Z. \tag{9}$$

Hence, we have

$$\frac{\partial \Phi(X, Y, Z, t)}{\partial t} = \frac{\partial \Phi(x, y, z, t)}{\partial t} - \frac{\partial \Phi}{\partial x}\,\dot{f}(t). \tag{10}$$

Let us introduce a new velocity potential ϕ by subtracting the velocity potential of the container $x\dot{f}(t)$ from Φ i.e.,

$$\phi = \Phi - x\dot{f}(t). \tag{11}$$

The potential describes the liquid motion relative to the moving container. Expressing Φ in terms of ϕ and using equation (5), one can transform equation (8) to

$$p_l = p_0 - \rho_f \left\{ \frac{\partial \phi}{\partial t} + g\varepsilon(R_M(0) - R\cos\theta) + R\sin\theta\cos\varphi\,\ddot{f}(t) + \tfrac{1}{2}(\nabla\phi)^2 + \dot{G}(t) \right\}. \tag{12}$$

Substituting equation (12) into equation (7) and applying the variation to each term leads to

$$\int_{t_1}^{t_2}\left\{\iiint_V \delta p_l \,\mathrm{d}V + \iiint_V (p_l - p_g)\,\delta(\mathrm{d}V) - \iint_F \sigma\delta(\mathrm{d}F)\right\}\mathrm{d}t$$
$$= \int_{t_1}^{t_2}\left[(-\rho_f)\iiint_V \left\{\delta\left(\frac{\partial\phi}{\partial t}\right) + \nabla\phi\cdot\delta(\nabla\phi) + \delta\dot{G}\right\}\mathrm{d}V\right.$$
$$\left. + \iiint_V (p_l - p_g)\,\delta(\mathrm{d}V) - \iint_F \sigma\delta(\mathrm{d}F)\right]\mathrm{d}t = 0. \tag{13}$$

It should be noted that the variation must be considered with respect to volume element $\mathrm{d}V$ and surface element $\mathrm{d}F$ as well as with respect to the liquid pressure p_l. For further transformation of equation (13), variation and differentiation may be transposed and the following relations hold:

$$\iiint_V \frac{\partial(\delta\phi)}{\partial t}\mathrm{d}V = \frac{\partial}{\partial t}\iiint_V \delta\phi\,\mathrm{d}V + \iint_F \frac{\partial\zeta}{\partial t}\cos\gamma_F\,\delta\phi\,\mathrm{d}F, \tag{14}$$

$$\iiint_V \frac{\partial(\delta G)}{\partial t}\mathrm{d}V = \frac{\partial}{\partial t}\iiint_V \delta G\,\mathrm{d}V + \iint_F \frac{\partial\zeta}{\partial t}\cos\gamma_F\,\delta G\,\mathrm{d}F, \tag{15}$$

$$\iiint_V \nabla\phi\cdot\nabla(\delta\phi)\,\mathrm{d}V = -\iint_F \nabla\phi\cdot\mathbf{N}_F\delta\phi\,\mathrm{d}F + \iint_W \nabla\phi\cdot\mathbf{N}_W\delta\phi\,\mathrm{d}W - \iiint_V \nabla^2\phi\,\delta\phi\,\mathrm{d}V, \tag{16}$$

$$\delta(\mathrm{d}V) = \mathrm{d}(\delta V) = -\delta\zeta\cos\gamma_F\,\mathrm{d}F, \tag{17}$$

$$\delta(\mathrm{d}F) = \mathrm{div}\,\mathbf{N}_F\,\delta\zeta\cos\gamma_F\,\mathrm{d}F\,. \tag{18}$$

Equations (14) and (15) arise from the fact that the time derivative of an integral over a time-varying domain (the first term on the right-hand side of each equation) is equal to the sum of an integral of the time derivative of the integrand over the instantaneous domain (the left-hand side of each equation) and an integral of the outward flux of the integrand over the moving boundary surface. Equation (16) can be derived by use of Green's theorem. Equation (17) can be understood from the fact that the variation of the liquid domain is due to the virtual liquid surface displacement in the direction normal to the liquid surface. The derivation of equation (18) is explained in Appendix A.

Substituting equations (14)–(18) into equation (13) and noting that $\delta\phi = \delta\zeta = 0$ at the time integration limits $t = t_1$ and t_2, one obtains

$$\int_{t_1}^{t_2}\left[\rho_f\left\{\iiint_V \nabla^2\phi\delta\phi\,\mathrm{d}V - \iint_W \nabla\phi\cdot\mathbf{N}_W\delta\phi\,\mathrm{d}W - \delta G\iint_F \frac{\partial\zeta}{\partial t}\cos\gamma_F\,\mathrm{d}F\right.\right.$$
$$\left.\left. - \iint_F\left(\frac{\partial\zeta}{\partial t}\cos\gamma_F - \nabla\phi\cdot\mathbf{N}_F\right)\delta\phi\,\mathrm{d}F\right\} + \iint_F (p_g - p_l - \sigma\,\mathrm{div}\,\mathbf{N}_F)\cos\gamma_F\,\delta\zeta\,\mathrm{d}F\right]\mathrm{d}t = 0. \tag{19}$$

Since the variations $\delta\phi$, $\delta\zeta$ and δG are arbitrary and independent of one another, equation (19) yields the following equations:

$$V\colon\ \nabla^2\phi = 0, \tag{20}$$

$$W\colon \nabla\phi\cdot\mathbf{N}_W = 0, \tag{21}$$

$$F: \begin{cases} p_g - p_l = \sigma \operatorname{div} \mathbf{N}_F, & (22) \\ (\partial\zeta/\partial t)\cos\gamma_F = \nabla\phi \cdot \mathbf{N}_F, & (23) \end{cases}$$

$$\iint_F (\partial\zeta/\partial t)\cos\gamma_F \, \mathrm{d}F = 0. \tag{24}$$

The Laplace equation (20) corresponds to the condition of continuity within the liquid domain. Equation (21) means that the liquid velocity in the direction normal to the rigid wall vanishes. Equations (22) and (23) present the dynamic and kinematic boundary conditions on the liquid surface, respectively. Equation (24) shows that the liquid volume is constant since the liquid is assumed to be incompressible. Since equation (24) can be derived from the other kinematic conditions (20), (21) and (23), equations (20)–(23) constitute the system of basic equations which governs low-gravity sloshing. In the following analysis using the Galerkin method, the combined and integrated form [equations (19)] is more convenient than the separated form [equations (20)–(24)].

We should note that the variational principle does not include the contact line condition which requires that the contact angle between liquid surface and container wall remains constant during sloshing. Hence, we must determine the admissible function for the liquid surface displacement by considering the contact line condition geometrically [equation (56) and Appendix C].

2.4. The Variational Principle in Spherical Coordinates

To solve the sloshing problem for an axisymmetrical container, it appears most convenient to express equation (19) in terms of the spherical coordinate system introduced in Section 2.2. The unit normal vectors, the surface elements and $\cos\gamma_F$ can be expressed as functions of $R_F(\theta, \varphi, t)$ and $R_W(\theta)$ and their θ- and φ-derivatives:

$$\mathbf{N}_F = \varepsilon(\mathbf{e}_R R_F \sin\theta - \mathbf{e}_\theta R_{F\theta}\sin\theta - \mathbf{e}_\varphi R_{F\varphi})/\{(R_F^2 + R_{F\theta}^2)\sin^2\theta + R_{F\varphi}^2\}^{1/2}, \tag{25}$$

$$\mathbf{N}_W = \varepsilon(\mathbf{e}_R R_W - \mathbf{e}_\theta R_{W\theta})/(R_W^2 + R_{W\theta}^2)^{1/2}, \tag{26}$$

$$\mathrm{d}F = R_F\{(R_F^2 + R_{F\theta}^2)\sin^2\theta + R_{F\varphi}^2\}^{1/2}\,\mathrm{d}\theta\,\mathrm{d}\varphi, \tag{27}$$

$$\mathrm{d}W = R_W(R_W^2 + R_{W\theta}^2)^{1/2}\sin\theta\,\mathrm{d}\theta\,\mathrm{d}\varphi, \tag{28}$$

$$\cos\gamma_F = \mathbf{N}_F \cdot \mathbf{e}_R = \varepsilon R_F \sin\theta/\{(R_F^2 + R_{F\theta}^2)\sin^2\theta + R_{F\varphi}^2\}^{1/2}. \tag{29}$$

Equations (25) and (26) can be derived from equations (2) and (3) by using the theorem that the normal vector of a surface expressed in the form $f(R, \theta, \varphi, t) = 0$ is given by grad f. Equation (27) can be obtained by determining the position vectors of the surface F,

$$\mathbf{X}_F(\theta, \varphi, t) = R_F(\theta, \varphi, t)\,(\mathbf{i}\sin\theta\cos\varphi + \mathbf{j}\sin\theta\sin\varphi + \mathbf{k}\cos\theta), \tag{30}$$

and estimating the area of the parallelogram formed by the infinitesimal tangential vectors along the θ- and φ-direction by

$$\mathrm{d}F = |\partial\mathbf{X}_F/\partial\theta \times \partial\mathbf{X}_F/\partial\varphi|\,\mathrm{d}\theta\,\mathrm{d}\varphi. \tag{31}$$

Substituting equations (25)–(29) into equation (19) and using the linear approximation, one obtains

$$
\begin{aligned}
&\rho_f \int_0^{2\pi}\int_0^{\bar\theta}\varepsilon\int_{R_M}^{R_W} \nabla^2\phi\delta\phi R^2\sin\theta \mathrm{d}R\,\mathrm{d}\theta\,\mathrm{d}\varphi \\
&-\rho_f\int_0^{2\pi}\int_0^{\bar\theta}\varepsilon\left(\frac{\partial\phi}{\partial R}\bigg|_{R=R_W}-\frac{R_{W\theta}}{R_W^2}\,\frac{\partial\phi}{\partial\theta}\bigg|_{R=R_W}\right)\delta\phi\bigg|_{R=R_W} R_W^2\sin\theta\,\mathrm{d}\theta\,\mathrm{d}\varphi \\
&-\rho_f\int_0^{2\pi}\int_0^{\bar\theta}\varepsilon\left(\frac{\partial\zeta}{\partial t}-\frac{\partial\phi}{\partial R}\bigg|_{R=R_M}+\frac{R_{M\theta}}{R_M^2}\,\frac{\partial\phi}{\partial\theta}\bigg|_{R=R_M}\right)\delta\phi\bigg|_{R=R_M} R_M^2\sin\theta\,\mathrm{d}\theta\,\mathrm{d}\varphi \\
&+\int_0^{2\pi}\int_0^{\bar\theta}\Bigg[\varepsilon(p_g-p_0)+\rho_f g\{R_M(0)-R_M\cos\theta\}-\sigma S_{0M}(\theta) \\
&+\varepsilon\rho_f\frac{\partial\phi}{\partial t}\bigg|_{R=R_M}-\rho_f g\zeta\cos\theta+\varepsilon\rho_f\ddot f(t)R_M\sin\theta\cos\varphi \\
&-\sigma\left\{S_{1M}(\theta)\zeta+S_{2M}(\theta)\frac{\partial\zeta}{\partial\theta}+S_{3M}(\theta)\frac{\partial^2\zeta}{\partial\theta^2}+S_{4M}(\theta)\frac{\partial^2\zeta}{\partial\varphi^2}\right\}\Bigg]\delta\zeta R_M^2\sin\theta\,\mathrm{d}\theta\,\mathrm{d}\varphi=0,
\end{aligned}
\tag{32}
$$

where

$$
\begin{aligned}
S_{0M}(\theta) &= R_M^{-1}(R_M^2+R_{M\theta}^2)^{-3/2} \\
&\quad\times\{2R_M^3+3R_MR_{M\theta}^2-R_M^2R_{M\theta\theta}-R_{M\theta}(R_M^2+R_{M\theta}^2)\cot\theta\}, \\
S_{1M}(\theta) &= R_M^{-2}(R_M^2+R_{M\theta}^2)^{-5/2} \\
&\quad\times\{-2R_M^5-5R_M^3R_{M\theta}^2+2R_M^4R_{M\theta\theta}-R_M^2R_{M\theta}^2R_{M\theta\theta} \\
&\quad+R_{M\theta}(2R_M^4+3R_M^2R_{M\theta}^2+R_{M\theta}^4)\cot\theta\}, \\
S_{2M}(\theta) &= R_M^{-1}(R_M^2+R_{M\theta}^2)^{-5/2} \\
&\quad\times\{3R_MR_{M\theta}(R_MR_{M\theta\theta}-R_{M\theta}^2)-R_M^2(R_M^2+R_{M\theta}^2)\cot\theta\}, \\
S_{3M}(\theta) &= -R_M(R_M^2+R_{M\theta}^2)^{-3/2}, \\
S_{4M}(\theta) &= -(\sin\theta)^{-2}R_M^{-1}(R_M^2+R_{M\theta}^2)^{-1/2}.
\end{aligned}
\tag{33}
$$

In the subsequent analysis, equation (32) is used as the basic equation for determining the eigenfrequency and estimating the liquid surface displacement and the slosh force and moment.

2.5. Slosh Force and Moment

The slosh force and moment are calculated by integrating the appropriate components of the liquid pressure, equation (12), and the surface tension over the wetted surface of the container wall and the contact line, respectively, i.e.

$$
F_x=F_{x1}+F_{x2}+F_{x3},\qquad M_y=M_{y1}+M_{y2}+M_{y3},
\tag{34}
$$

where

$$F_{x1} = \iint_W P_D(\mathbf{N}_W \cdot \mathbf{i})\,\mathrm{d}W,$$
$$M_{y1} = \iint_W P_D\{(\mathbf{N}_W \cdot \mathbf{i})\,z - (\mathbf{N}_W \cdot \mathbf{k})x\}\mathrm{d}W; \tag{35}$$

$$F_{x2} = \varepsilon \int_C (p_g - p_c)\zeta(\mathbf{N}_W \cdot \mathbf{i})\mathrm{d}C,$$
$$M_{y2} = \varepsilon \int_C (p_g - p_c)\zeta\{(\mathbf{Nw} \cdot \mathbf{i})z - (\mathbf{N}_W \cdot \mathbf{k})x\}\,\mathrm{d}C; \tag{36}$$

$$F_{x3} = \sigma \int_C (\mathbf{t}_F \cdot \mathbf{i})\,\mathrm{d}C,$$
$$M_{y3} = \sigma \int_C \{(\mathbf{t}_F \cdot \mathbf{i})z - (\mathbf{t}_F \cdot \mathbf{k})x\}\,\mathrm{d}C. \tag{37}$$

The slosh moment is about the tank bottom ($z = 0$). Note that three kinds of force and moment, equations (35)–(37), arise as indicated by equation (34). First, equation (35) gives the force and moment due to the linearized dynamic liquid pressure which is written from equation (12) as

$$P_D = -\rho_f \{\partial\phi/\partial t + R\sin\theta\cos\varphi \ddot{f}(t)\}. \tag{38}$$

Second, equation (36) indicates the force and moment exerted along the contact line C caused by the pressure difference across the liquid–gas interface. These are created from the fact that when the wetted region is increased due to the liquid surface displacement, the areas exposed to p_g and p_l decrease and increase, respectively, and p_g is larger than p_l at the interface. Third, equation (37) represents the force and moment caused by the unbalanced pull of the surface tension σ at the moving contact line C, i.e. $\mathbf{t}_F$ is the unit vector perpendicular to the contact line C and parallel to the oscillating liquid surface F:

$$\mathbf{t}_F = \{\mathbf{N}_F \times (\mathbf{N}_F \times \mathbf{N}_W)\} / |\mathbf{N}_F \times (\mathbf{N}_F \times \mathbf{N}_W)|. \tag{39}$$

2.6. Dimensionless Parameters

For convenience in the subsequent analysis and numerical calculation, dimensionless quantities are introduced here. Letting b^* be the characteristic length and defining the characteristic frequency by

$$\omega_g^* = \sqrt{g^*/b^*}, \tag{40}$$

the following dimensionless quantities can be introduced:

$$\phi = \phi^*/(b^*)^2\omega_g^*, \quad \zeta = \zeta^*/b^*,$$
$$\{R, R_M(\theta), R_W(\theta)\} = (R^*, R_M^*(\theta), R_W^*(\theta)\}/b^*, \quad t = \omega_g^* t^*, \quad \ddot{f}(t) = \ddot{f}^*(t^*)/b^*(\omega_g^*)^2,$$
$$\{S_{1M}, S_{2M}, S_{3M}, S_{4M}\} = (b^*)^2\{S_{1M}^*, S_{2M}^*, S_{3M}^*, S_{4M}^*\},$$
$$P_D = P_D^*/\rho_f^*(b^*)^2(\omega_g^*)^2, \quad \{\mathrm{d}F, \mathrm{d}W\} = \{\mathrm{d}F^*, \mathrm{d}W^*\}/(b^*)^2, \tag{41}$$

$$F_x = F_x^*/\rho_f^*(b^*)^4(\omega_g^*)^2, \quad M_y = M_y^*/\rho_f^*(b^*)^5(\omega_g^*)^2, \tag{42}$$

$$\omega = \omega^*/\omega_g^*, \tag{43}$$

$$\mathrm{Bo} = \rho_f^* g^*(b^*)^2/\sigma^*. \tag{44}$$

Note that dimensional quantities are distinguished from the corresponding nondimensional ones by adding an asterisk; i.e. an asterisk should be added to all dimensional quantities, which have been used hitherto. Equation (44) defines the Bond number Bo, which is the dimensionless parameter relating the magnitude of gravity to surface tension.

3. DETERMINATION OF MODAL FUNCTIONS

As a preliminary step to the forced vibration analysis, the modal functions for ϕ and ζ are determined by a free vibration analysis, where the excitation $\bar{f}(t)$ is omitted in the variational principle (32). The frequency equation is derived in the form of a standard eigenvalue problem by analytical procedures.

3.1. Solution of the Laplace Equation in Spherical Coordinates

In spherical coordinates, the Laplace equation (20) becomes

$$\nabla^2\phi \equiv \frac{\partial^2\phi}{\partial R^2} + \frac{2}{R}\frac{\partial\phi}{\partial R} + \frac{1}{R^2}\frac{\partial^2\phi}{\partial\theta^2} + \frac{\cot\theta}{R^2}\frac{\partial\phi}{\partial\theta} + \frac{1}{R^2\sin^2\theta}\frac{\partial^2\phi}{\partial\varphi^2} = 0. \tag{45}$$

The solution of equation (45) must be expressed by a linear combination of characteristic functions whose orthogonality is satisfied within the range $0 \leqq \theta \leqq \bar{\theta}$. Since $\bar{\theta} < \pi/2$ (see Figure 1), such orthogonality cannot be satisfied by the associated Legendre functions. This is the reason why the characteristic functions must be derived anew here. We assume a solution in terms of separated variables, i.e.

$$\phi(R, \theta, \varphi, t) = X(R)\Theta(\theta)\cos m\varphi \mathrm{e}^{\mathrm{i}\omega t}. \tag{46}$$

Substitution of equation (46) into equation (45) gives

$$R^2\frac{\mathrm{d}^2X}{\mathrm{d}R^2} + 2R\frac{\mathrm{d}X}{\mathrm{d}R} - \lambda X = 0, \tag{47}$$

$$\frac{\mathrm{d}^2\Theta}{\mathrm{d}\theta^2} + \cot\theta\frac{\mathrm{d}\Theta}{\mathrm{d}\theta} - \frac{m^2}{\sin^2\theta}\Theta + \lambda\Theta = 0, \tag{48}$$

where λ denotes the characteristic value to be determined later. Substituting $X = R^\alpha$ into equation (47), one obtains

$$\alpha(\alpha + 1) - \lambda = 0. \tag{49}$$

On the other hand, equation (48) is solved for the boundary condition

$$\left.\frac{\mathrm{d}\Theta}{\mathrm{d}\theta}\right|_{\theta = \bar{\theta}} = 0. \tag{50}$$

This can be derived by considering the limit $\theta \to \bar{\theta}$ of the boundary condition on the container wall given by

$$\left(\frac{\partial \phi}{\partial R} - \frac{R_{W\theta}}{R_W^2}\frac{\partial \phi}{\partial \theta}\right)_{R = R_W(\theta)} = 0, \quad 0 \leqq \theta \leqq \bar{\theta}, \tag{51}$$

which can be found from the second term of the variational principle (32). Let us consider the derivation of equation (50) from equation (51) in more detail. Equation (51) can be rewritten as

$$\left(\frac{1}{R_{W\theta}}\frac{\partial \phi}{\partial R} - \frac{1}{R_W^2}\frac{\partial \phi}{\partial \theta}\right)_{R = R_W(\theta)} = 0. \tag{52}$$

When θ approaches $\bar{\theta}$, $|R_{W\theta}|$ tends towards ∞ (see Figure 1), so that the first term of equation (52) becomes negligible. The remaining second term tends towards the boundary condition (50), as can be seen from equation (46). Thus, the boundary condition for the characteristic function $\Theta(\theta)$ can be determined by the kinematic condition at the contact line $\theta = \bar{\theta}$, i.e. only (50), instead of throughout the container wall, i.e. (51). Therefore, irrespective of the generatrix shape of the container, the characteristic function $\Theta(\theta)$ can be analytically determined by solving the boundary value problem constituted by equations (48) and (50). The kth characteristic function is given by

$$\begin{aligned}\Theta_k(\theta) &= (1-\xi^2)^{m/2} F(m-\alpha, \alpha+m+1, m+1, (1-\xi)/2) \\ &= (1-\xi^2)^{m/2} \sum_{i=0}^{\infty} \\ &\quad \times \frac{(m-\alpha)(m-\alpha+1)\cdots(m-\alpha+i-1)(\alpha+m+1)(\alpha+m+2)\cdots(\alpha+m+i)}{1\cdot 2\cdots i \times (m+1)(m+2)\cdots(m+i)} \\ &\quad \times \{(1-\xi)/2\}^i; \quad \xi = \cos\theta. \end{aligned} \tag{53}$$

Regarding the derivation of equation (53), refer to Appendix B.

Expressing $\Theta_k(\theta)$ in terms of the Gauss hypergeometric series is helpful for examining the convergence of the series solution. The Gauss hypergeometric series $F(\alpha, \beta, \gamma, x)$ converges for arbitrary values of α, β and γ, provided that $|x| < 1$. Hence, solution (53) converges for $0 \leqq \theta < \pi$. In the present analysis, we have $0 \leqq \theta \leqq \bar{\theta}$, where $\bar{\theta}$ cannot be larger than $\pi/2$ as can be seen from Figure 1. Therefore, convergence of solution (53) is assured.

The characteristic exponent α of the R-dependent function $X(R)$ is determined from equation (49) as

$$\alpha_{1k} = (-1 - \sqrt{1+4\lambda_k})/2, \quad \alpha_{2k} = (-1 + \sqrt{1+4\lambda_k})/2\,. \tag{54}$$

By linear combination of the characteristic functions, the velocity potential and the liquid surface displacement can be expressed as

$$\phi(R, \theta, \varphi, t) = \mathrm{i}\omega \sum_{k=1}^{\infty} \left\{ a_k \left(\frac{R}{l_a}\right)^{\alpha_{1k}} + b_k \left(\frac{R}{l_b}\right)^{\alpha_{2k}} \right\} \Theta_k(\theta) \cos m\varphi \, \mathrm{e}^{\mathrm{i}\omega t}, \tag{55}$$

$$\zeta(\theta, \varphi, t) = \sum_{k=1}^{\infty} c_k \Theta_k(\theta) \cos m\varphi \, \mathrm{e}^{\mathrm{i}\omega t}, \tag{56}$$

where a_k, b_k and c_k are arbitrary real constants and l_a and l_b are normalization parameters introduced for improving the convergence of series (55). Namely, with the increase of k, $\lambda_k \to \infty$, i.e. $\alpha_{1k} \to -\infty$ and $\alpha_{2k} \to \infty$ [see equation (54)], so that l_a and l_b are, respectively, the minimum and maximum of R considered, which is $R_M(\theta)$ and $R_W(\theta)$ $(0 \leqq \theta \leqq \bar{\theta})$.

Equation (56) is obtained by imposing

$$(\partial\zeta/\partial\theta)_{\theta=\bar{\theta}} = 0 \tag{57}$$

as a dynamical contact line condition. This is an approximate method, but it introduces a small error even for a small static contact angle θ_c, by virtue of the special way the spherical coordinates are used in the present study. More detailed discussion on this approximation is given in Appendix C.

3.2. Frequency Equation

To obtain the frequency equation, we substitute equations (55) and (56) into equation (32) and neglect the excitation term. Using the Galerkin method, considering variations with respect to a_k, b_k and c_k, and truncating the summation in equations (55) and (56) at $\bar{k}$, yields the following system of algebraic homogeneous equations:

$$\left(-\omega^2 \begin{bmatrix} \mathbf{M}_{aa} & \mathbf{M}_{ab} & \mathbf{M}_{ac} \\ \mathbf{M}_{ba} & \mathbf{M}_{bb} & \mathbf{M}_{bc} \\ \mathbf{M}_{ca} & \mathbf{M}_{cb} & \mathbf{0} \end{bmatrix} + \begin{bmatrix} \mathbf{0} & \mathbf{0} & \mathbf{0} \\ \mathbf{0} & \mathbf{0} & \mathbf{0} \\ \mathbf{0} & \mathbf{0} & \mathbf{K}_{cc} \end{bmatrix} \right) \begin{Bmatrix} \mathbf{a} \\ \mathbf{b} \\ \mathbf{c} \end{Bmatrix} = \{\mathbf{0}\}, \tag{58}$$

where $\mathbf{a}$, $\mathbf{b}$ and $\mathbf{c}$ are column vectors defined by

$$\mathbf{a} = \{a_1, a_2, \ldots, a_{\bar{k}}\}^{\mathrm{T}}, \quad \mathbf{b} = \{b_1, b_2, \ldots, b_{\bar{k}}\}^{\mathrm{T}}, \quad \mathbf{c} = \{c_1, c_2, \ldots, c_{\bar{k}}\}^{\mathrm{T}}, \tag{59}$$

and $\mathbf{M}_{aa}$, etc., are $\bar{k} \times \bar{k}$ matrices whose components are presented in Appendix D.

For reducing the dimension of the eigenvalue problem from $3\bar{k}$ [equation (58)] to $\bar{k}$, express $\mathbf{a}$ and $\mathbf{b}$ in terms of $\mathbf{c}$ as

$$\{\mathbf{a}\} = -[\mathbf{M}'_{aa}\mathbf{M}_{ac} + \mathbf{M}'_{ab}\mathbf{M}_{bc}]\{\mathbf{c}\}, \quad \{\mathbf{b}\} = -[\mathbf{M}'_{ba}\mathbf{M}_{ac} + \mathbf{M}'_{bb}\mathbf{M}_{bc}]\{\mathbf{c}\}, \tag{60}$$

where $\mathbf{M}'_{aa}$, $\mathbf{M}'_{ab}$, $\mathbf{M}'_{ba}$ and $\mathbf{M}'_{bb}$ are $\bar{k} \times \bar{k}$ matrices defined by

$$\begin{bmatrix} \mathbf{M}'_{aa} & \mathbf{M}'_{ab} \\ \mathbf{M}'_{ba} & \mathbf{M}'_{bb} \end{bmatrix} = \begin{bmatrix} \mathbf{M}_{aa} & \mathbf{M}_{ab} \\ \mathbf{M}_{ba} & M_{bb} \end{bmatrix}^{-1}. \tag{61}$$

Substitution of equation (60) into (58) yields the following standard eigenvalue problem with dimension $\bar{k}$:

$$[-\omega^2\mathbf{M} + \mathbf{K}]\{\mathbf{c}\} = \{\mathbf{0}\}, \tag{62}$$

where

$$\mathbf{M} = -\mathbf{M}_{ca}(\mathbf{M}'_{aa}\mathbf{M}_{ac} + \mathbf{M}'_{ab}\mathbf{M}_{bc}) - \mathbf{M}_{cb}(\mathbf{M}'_{ba}\mathbf{M}_{ac} + \mathbf{M}'_{bb}\mathbf{M}_{bc}), \quad \mathbf{K} = \mathbf{K}_{cc}. \tag{63}$$

From equation (62), ω can be determined as a solution of

$$|-\omega^2\mathbf{M} + \mathbf{K}| = 0. \tag{64}$$

The eigenvector $\mathbf{c}$ determined by equation (62) yields the eigenmodes of the liquid surface displacement ζ [equation (56)], while $\mathbf{a}$ and $\mathbf{b}$ calculated by equation (60) yield eigenmodes of the velocity potential ϕ [equation (55)].

The dimension $\bar{k}$ of the eigenvalue problem (62) for obtaining a sufficiently converged solution is small due to the orthogonality of the characteristic functions (53), so that the present analysis requires only a small amount of computation time and cost. The analytical derivation of the characteristic functions Θ_k and the rapid convergence of their constituting series [equation (53)] are helpful for fast computation.

4. RESPONSE TO LATERAL EXCITATION

The purpose of this section is to perform a forced vibration analysis using the modal functions determined in Section 3. First, the modal equation is derived by applying the Galerkin method to the variational principle (32) presented in this paper. Then, the liquid surface displacement and the slosh force and moment are determined by solving the modal equation.

4.1. Modal Equation

Since a lateral excitation causes only the mode with circumferential wave number $m = 1$, we may express ϕ and ζ in terms of their modal functions (55) and (56) with $m = 1$, i.e.

$$\phi = \dot{q}(t) \sum_{k=1}^{\infty} \left\{ a_k \left(\frac{R}{l_a} \right)^{\alpha_1 k} + b_k \left(\frac{R}{l_b} \right)^{\alpha_2 k} \right\} \Theta_k(\theta) \cos \varphi, \tag{65}$$

$$\zeta = q(t) \sum_{k=1}^{\infty} c_k \Theta_k(\theta) \cos \varphi, \tag{66}$$

where only the fundamental mode is considered, since this mode is of greatest importance in the resonant and critical case. The modal coordinate for the fundamental mode is denoted by $q(t)$. Substituting equations (65) and (66) into the variational principle (32) and considering the variation with respect to $q(t)$ leads to the following modal equation:

$$M\ddot{q} + Kq = \beta \ddot{f}(t), \tag{67}$$

where M, K and β are given in Appendix E. Equation (67) can be written as

$$\ddot{q} + \omega^2 q = \beta_1 \ddot{f}(t); \quad \omega^2 = K/M, \quad \beta_1 = \beta/M. \tag{68}$$

4.2. Slosh Force and Moment

One can express the slosh force and moment in terms of the modal coordinates $q(t)$ by substituting equations (65) and (66) into equation (34). In dimensionless form (Section 2.6) we finally obtain

$$F_x = A_1 \ddot{q}(t) + A_2 \ddot{f}(t) + A_3 q(t), \quad M_y = A_4 \ddot{q}(t) + A_5 \ddot{f}(t) + A_6 q(t). \tag{69}$$

Constants A_1–A_6 are not presented here for brevity.

5. NUMERICAL RESULTS

5.1. Meniscus Shape and Eigenfrequency

Figure 2 shows the meniscus shape for a spherical container and a contact angle of 5° between meniscus and container wall also shown in a previous paper (Utsumi 1988). It is

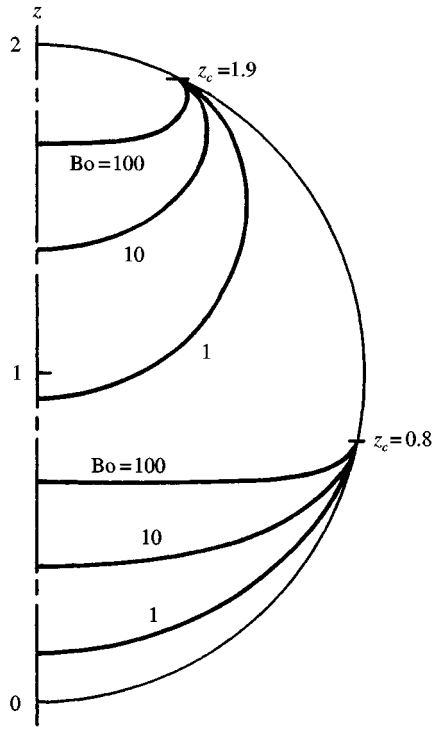

Figure 2. Shape of meniscus for various Bond numbers and dimensionless z-coordinates of contact line.

presented again in order to facilitate the discussion of the numerical results for eigenfrequency and displacement of the liquid surface given below. It can be seen that, when the Bond number Bo is large, the menisci are almost flat except in the vicinity of the container wall. With decreasing Bond number, the menisci tend more and more to exhibit spherical shapes. For the case Bo = 0, which corresponds to a zero-gravity environment, the menisci are exactly spherical (Utsumi 1989, Appendix D).

Figure 3 shows the dimensionless eigenfrequency ω [equation (43)] of the fundamental mode $m = 1$ for a spherical container. A considerable difference is found between the ω versus Bo relations for large z_c ($1{\cdot}5 < z_c$) and small z_c ($z_c < 0{\cdot}3$). Namely, for $1{\cdot}5 < z_C$, ω decreases drastically with decreasing Bo within the range $10 <$ Bo, whereas for $z_c < 0{\cdot}3$, ω increases remarkably with the reduction of Bo within Bo < 10. These results can be explained physically as follows. The volume-to-area ratio becomes large for $1{\cdot}5 < z_c$, so that the sloshing exhibits properties of a gravity wave rather than those of a surface tension wave for a fairly wide range of Bo. The natural frequency of the gravity wave increases with increasing liquid depth. A lower centre of the meniscus with smaller Bo (Figure 2) means a shallower liquid depth. Hence, ω decreases with decreasing Bo for $1{\cdot}5 < z_c$. On the other hand, for small $z_c (z_c < 0{\cdot}3)$, the sloshing exhibits properties of a surface tension wave. The potential energy due to surface tension is much larger than that due to gravity. Furthermore, it is to be noted that ω is nondimensionalized by the gravity [see equation (43) together with equation (40)], so that ω becomes large for small Bo. Assuming that $z_c \sim \mathcal{O}(\varepsilon)$ for the case of $z_c \to 0$, the liquid surface area decreases, according to the surface tension potential, as $\mathcal{O}(\varepsilon^2)$; this is a slower rate of decrease than the liquid volume, which according

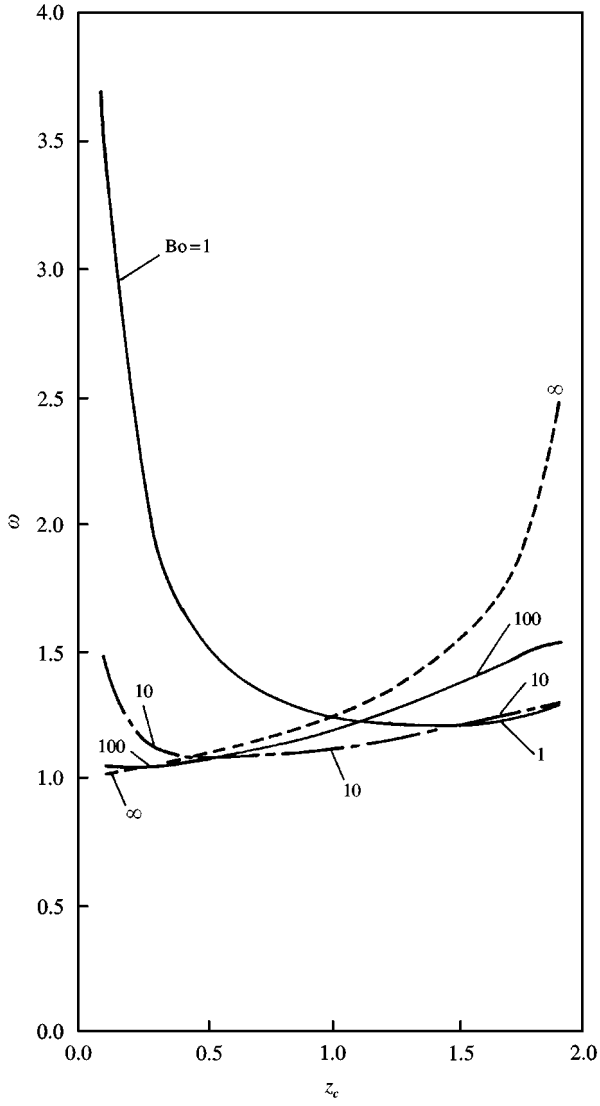

Figure 3. Dimensionless eigenfrequency $\omega = \omega^*/\sqrt{g^*/b^*}$; ω^* is the dimensional eigenfrequency, g^* the gravitational acceleration, and b^* the half-height of the container.

to the gravity potential, is $\mathcal{O}(\varepsilon^3)$. This is the reason why the surface tension effect prevails rather than the gravity effect for $z_c \to 0$, and ω increases drastically with $z_c \to 0$ and $\mathrm{Bo} \to 0$. In order to verify the discussion, it is useful to define another dimensionless eigenfrequency normalized by a quantity independent of g^*. Figure 4 shows the dimensionless eigenfrequency $\bar{\omega}$ defined by

$$\bar{\omega} = \omega^*/\omega_\sigma^*, \tag{70}$$

where

$$\omega_\sigma^* = \sqrt{\sigma^*/(\rho_f^* b^{*3})}. \tag{71}$$

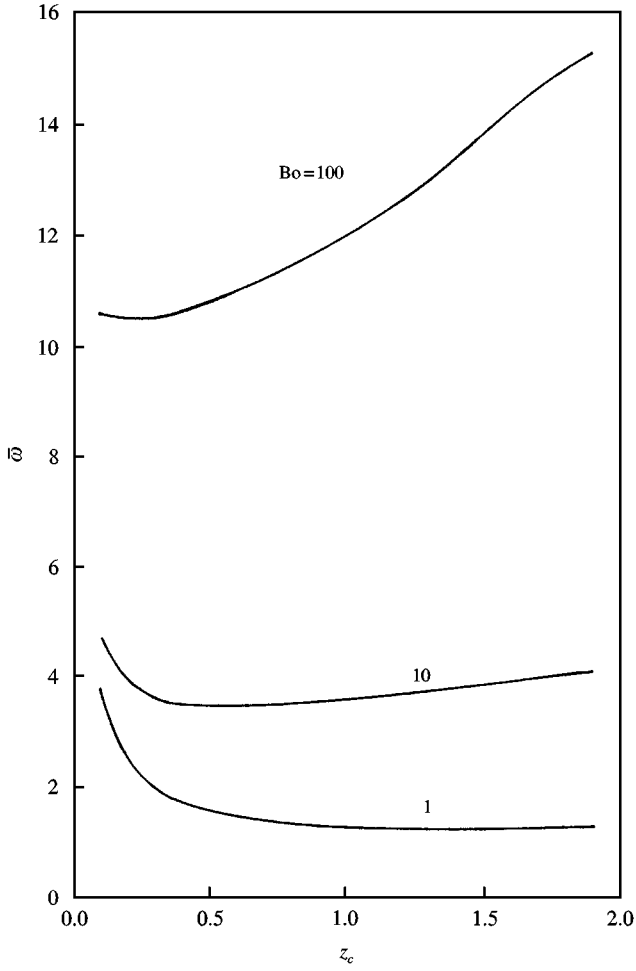

Figure 4. Alternative dimensionless eigenfrequency $\bar{\omega} = \omega^*/\sqrt{\sigma^*/\rho_f^*(b^*)^3}$; ω^* is the dimensional eigenfrequency, σ^* the surface tension, ρ_f^* the liquid density, and b^* the half-height of the container.

The value of $\bar{\omega}$ can be calculated from the formerly defined dimensionless eigenfrequency ω given by equation (43); i.e.

$$\bar{\omega} = \omega\sqrt{\mathrm{Bo}}\,. \tag{72}$$

It can be seen that for small z_c the $\bar{\omega}$ versus Bo relationship is different from that of ω versus Bo, i.e. $\bar{\omega}$ does not increase with decreasing Bond number.

Figure 5 compares eigenfrequencies obtained by the present analysis with experimental results (Dodge & Garza 1970). Good agreement is obtained.

5.2. Response to Lateral Excitation

Figure 6 shows the amplitude of the stationary response of the dimensionless liquid surface displacement ζ at the container wall $(\theta, \varphi) = (\bar{\theta}, 0)$ and the lateral slosh force F_x and moment

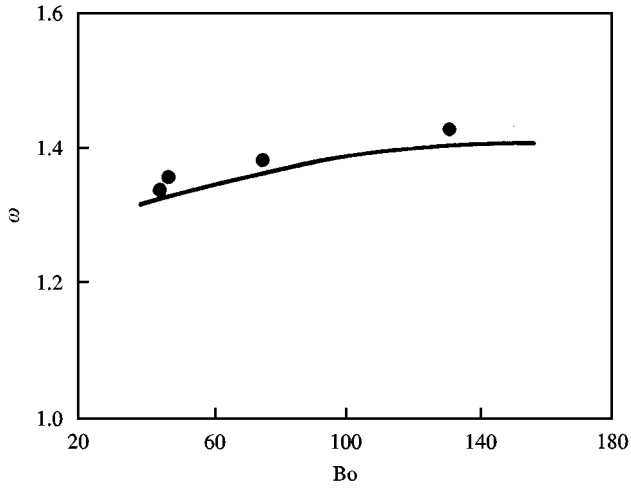

Figure 5. Dimensional eigenfrequency ω versus the Bond number Bo: ——, present analysis; ●, experiment by Dodge & Garza (1970). Liquid volume/container volume is 0·85.

M_y for a spherical container subjected to sinusoidal lateral acceleration of amplitude $0{\cdot}0125g^*$ and angular frequency $0{\cdot}95\ \omega^*$. This is a critical case where the excitation frequency is near the eigenfrequency ω^* of the fundamental mode. The modal damping is assumed to be 0·01.

First, it can be seen from Figure 6 (a) that the influence of Bo on the amplitude of the dimensionless liquid surface displacement ζ changes for liquid-filling levels larger than, say, $z_c = 1$. Namely, we find that (i) for small z_c (approximately $0 < z_c < 1$), ζ increases with increasing Bo, and that (ii) for large z_c (approximately $1 < z_c < 2$), ζ becomes maximal for a certain finite value of Bo.

Result (ii) signifies that the analysis for $\mathrm{Bo} \to \infty$, which does not take into consideration the surface tension effect at all, underestimates the liquid surface oscillation for $1 < z_c < 2$. Such an underestimation is serious for a liquid-filling level close to 2. In addition, for $z_c \to 2$ the range of Bo that makes ζ larger than ζ for $\mathrm{Bo} \to \infty$ becomes wider as shown by the dashed line in Figure 6 (a). We attribute the reason to the remarkable increase of ω^{-2} (Figure 3) and the absolute value of the factor

$$\beta_k = \int_0^{\bar{\theta}} R_M^3 \sin^2\theta \Theta_k \, \mathrm{d}\theta \tag{73}$$

with the decrease of Bo from infinity. The factor appears in the excitation parameter β [equation (E3) in Appendix E] of the modal equation (67) and becomes much larger in magnitude for a finite Bond number than an infinite one for the following reason. In equation (73), R_M is the distance between an arbitrary point on the meniscus and the origin, i.e. the top of the cone tangential to the container at the contact line $z = z_c$ (Figure 1). Therefore, as can be seen from Figure 2, R_M is much larger for finite Bond number than for infinite Bond number, for which the meniscus is the plane $z = z_c$. It should be noted here that the large difference in R_M for finite and infinite Bond numbers is due to the very small contact angle between the meniscus and the container wall (Neu & Good 1963) and the large tilt of the container wall from the vertical direction (i.e. parallel to the z-axis) near

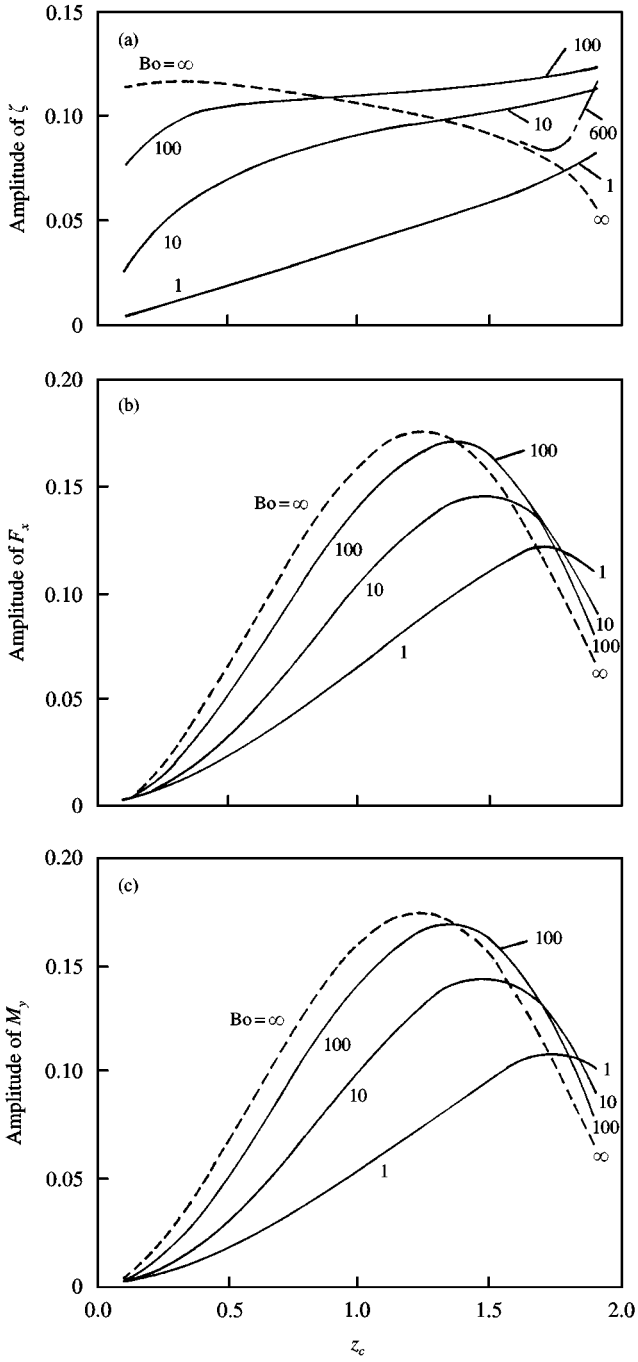

Figure 6. Amplitude of stationary response to sinusoidal lateral excitation in the x-direction of amplitude 0·0125 g* and angular frequency 0·95ω* (modal damping ratio is 0·01): (a) dimensionless liquid surface displacement ζ at the container wall; (b) dimensionless slosh force F_x exerted to the container; (c) dimensionless slosh moment M_y exerted to the container.

$z = 2$. This difference is accentuated by the fact that R_M is raised to the third power in equation (73).

The responses of dimensionless slosh force F_x and moment M_y are shown in Figures 6(b) and 6(c), respectively. First, let us consider the physical meanings of the results for $\mathrm{Bo} \to \infty$ and $\mathrm{Bo} = 100$, where F_{x1} and M_{y1} in equation (34) prevail over the other terms. In this case, note that F_x and M_y are close to each other since the relation

$$F_{x1} = M_{y1} \tag{74}$$

holds for a spherical container. This is because both the force and moment acting on the surface element of the container wall are equal to $\mathrm{d}F_{x1} = \mathrm{d}M_{y1} = P_D \sin\psi \cos\varphi \, \mathrm{d}W$, where ψ denotes the angle between the normal of W and the z-axis at the position (θ, φ) and the container radius can be considered as unity since it has been used for nondimensionalization [equation (42)]. The magnitude of the dynamic pressure P_D along the container wall is maximal at the liquid surface ($z = z_c$). Hence, the resultant slosh force and moment are determined mainly by the pressure near the liquid surface. The pressure is exerted on the container wall in its normal direction and both the x-component of $\mathbf{N}_W$ and the distance between $\mathbf{N}_W$ and the moment centre (y-axis) at the position $(z, \varphi) = (z_c, 0)$ are maximal at $z_c = 1$, i.e. just at the mid-filling level. Therefore, F_x and M_y do not necessarily increase monotonically with the filling level z_c but exhibit a maximum at a certain intermediate value of z_c. The value of z_c giving the maximum of F_x and M_y becomes somewhat higher than $z_c = 1$ due to the following two factors: (a) increasing z_c extends the wetted region of the container wall subjected to the liquid pressure; (b) with increasing z_c, the liquid surface displacement increases [Figure 6 (a)] except for very large Bond number. Due to the second factor, the z_c giving the maximum slosh force and moment is larger for $\mathrm{Bo} = 100$ than for $\mathrm{Bo} \to \infty$.

For smaller Bond numbers ($\mathrm{Bo} = 10$ and 1), F_{x2}, M_{y2}, F_{x3}, and M_{y3} in equation (34) become important. Due to F_{x3} and M_{y3}, the relation $F_x = M_y$ no longer holds and the z_c yielding the maximum F_x and M_y shifts to higher values with decreasing Bo, since the second influence mentioned above becomes important.

Figure 7 shows the dimensionless slosh force and moment alternatively defined as

$$\bar{F}_x = F_x^* / \rho_f^* (b^*)^4 (\omega_\sigma^*)^2, \quad \bar{M}_y = M_y^* / \rho_f^* (b^*)^5 (\omega_\sigma^*)^2, \tag{75}$$

which can be calculated from the formerly defined dimensionless slosh force and moment by [cf. equation (42)]

$$\bar{F}_x = F_x \mathrm{Bo}, \quad \bar{M}_y = M_y \mathrm{Bo}. \tag{76}$$

5.3. Convergence of Numerical Results

Examples for the convergence of the numerical results with increasing dimension $\bar{k}$ for the eigenvalue problem (62) are shown in Tables 1–3, which are, respectively, for the eigenfrequency, liquid surface displacement and slosh force. The percentage figures express the ratio of the result for arbitrary $\bar{k}$ and $\bar{k} = 10$, which is supposed here to be close to the exact solution. The convergence becomes slower for smaller Bond numbers and lower liquid-filling levels, for which the meniscus is thin (Figure 2) and the ratio between the liquid and container volumes very small (e.g. 5·9% for $\mathrm{Bo} = 10$ and $z_c = 0{\cdot}5$). In such a case, the slosh

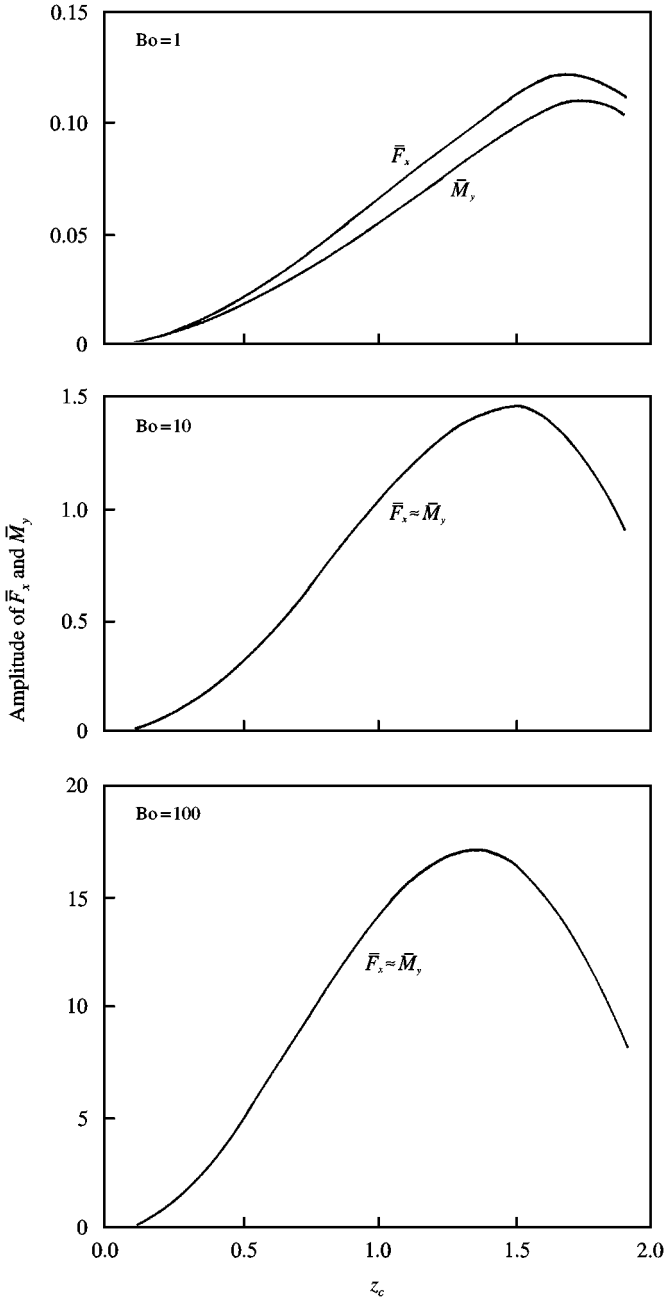

Figure 7. Amplitude of alternative dimensionless slosh force and moment.

force and moment are no longer an important factor for vehicle control (Figure 6) and are negligible for engineering purposes. The computation time is only 10 s for $\bar{k} = 10$ and decrease with $\bar{k}^2$. Thus, the present analytical method requires a small amount of computation time and cost.

TABLE 1
Convergence of numerical result for eigenfrequency with increasing dimension of eigenvalue problem; all entries in the table are in percent (%)

(a) Bo = 1				(b) Bo = 10			
$\bar{k}$	$z_c = 0{\cdot}5$	$z_c = 1{\cdot}1$	$z_c = 1{\cdot}7$	$\bar{k}$	$z_c = 0{\cdot}5$	$z_c = 1{\cdot}1$	$z_c = 1{\cdot}7$
1	123·7	109·8	108·6	1	106·9	101·9	101·9
2	108·3	102·5	101·2	2	102·5	100·9	100·8
3	104·9	101·5	100·6	3	101·4	100·5	100·3
4	103·1	101·0	100·4	4	100·9	100·3	100·2
5	102·1	100·7	100·3	5	100·6	100·2	100·1
6	101·4	100·5	100·2	6	100·4	100·1	100·1
7	100·9	100·3	100·1	7	100·2	100·1	100·1
8	100·5	100·2	100·1	8	100·1	100·1	100·0
9	100·3	100·1	100·0	9	100·1	100·0	100.0
10	100·0	100·0	100·0	10	100·0	100·0	100·0
(c) Bo = 100				(d) Bo $\to \infty$			
1	101·8	100·7	104·1	1	101·3	100·4	104·4
2	100·6	100·3	101·2	2	100·4	100·2	101·7
3	100·3	100·2	100·4	3	100·2	100·1	100·9
4	100·2	100·1	100·2	4	100·1	100·1	100·5
5	100·1	100·1	100·1	5	100·1	100·1	100·3
6	100·1	100·1	100·1	6	100·1	100·0	100·2
7	100·1	100·1	100·1	7	100·0	100·0	100·1
8	100·0	100·0	100·0	8	100·0	100·0	100·1
9	100·0	100·0	100·0	9	100·0	100·0	100·0
10	100.0	100·0	100·0	10	100·0	100·0	100·0

6. CONCLUSIONS

The response of the low-gravity propellant sloshing has been analysed for the case where an axisymmetrical container is exposed to lateral excitation. The results can be summarized as follows.

(a) Using the spherical coordinate system with its origin at the top of the cone tangential to the container at the contact line of the meniscus with the container wall enables us (i) to analytically derive the characteristic functions for an arbitrary axisymmetrical convex container, (ii) to express the liquid surface and its dynamical displacement as a single-valued function and (iii) to satisfy the compatibility condition for the liquid surface displacement at the container wall.

(b) A variational principle taking into account the surface tension as well as the resulting pressure difference on the liquid–gas interface has been introduced.

(c) As a preliminary step to the response analysis, eigenfrequencies and modal functions have been determined. The variational principle has been transformed to a frequency equation by the Galerkin method, constituting a standard eigenvalue problem. The characteristic functions have been expressed analytically in terms of the Gauss hypergeometric series for an arbitrary axisymmetrical container rather than by conventional numerical methods. Since the characteristic functions are determined analytically and the dimension

TABLE 2
Convergence of numerical result for liquid surface displacement with increasing dimension of eigenvalue problem; all entries in the table are in percent (%)

(a) Bo = 1				(b) Bo = 10			
$\bar{k}$	$z_c = 0{\cdot}5$	$z_c = 1{\cdot}1$	$z_c = 1{\cdot}7$	$\bar{k}$	$z_c = 0{\cdot}5$	$z_c = 1{\cdot}1$	$z_c = 1{\cdot}7$
1	54·8	77·1	92·5	1	73·5	88·9	92·6
2	69·6	85·9	96·3	2	83·3	93·2	97·6
3	78·1	90·2	97·6	3	88·5	95·5	98·7
4	84·0	93·0	98·4	4	91·7	96·9	99·3
5	88·3	94·9	98·9	5	94·0	97·7	99·5
6	91·6	96·4	99·2	6	95·7	98·4	99·7
7	94·3	97·6	99·5	7	97·1	98·9	99·8
8	96·5	98·5	99·7	8	98·2	99·3	99·9
9	98·4	99·3	99·9	9	99·2	99·7	100·0
10	100·0	100·0	100·0	10	100·0	100·0	100·0
(c) Bo = 100				(d) Bo $\rightarrow \infty$			
1	83·1	92·3	82·8	1	83·9	99·7	106·2
2	90·8	96·1	93·2	2	91·9	100·1	100·7
3	94·1	97·6	97·3	3	95·2	100·1	99·7
4	96·0	98·3	98·9	4	96·9	100·1	99·4
5	97·2	98·8	99·5	5	98·0	100·1	99·3
6	98·0	99·2	99·7	6	98·6	100·1	99·3
7	98·7	99·5	99·8	7	99·1	100·1	99·4
8	99·2	99·7	99·9	8	99·5	100·0	99·6
9	99·6	99·9	100·0	9	99·8	100·0	99·8
10	100·0	100·0	100·0	10	100·0	100·0	100·0

of the eigenvalue problem for obtaining sufficiently converged results is low, the present method requires only a small amount of computation time and cost.

(d) For calculating the response to lateral excitation, the variational principle has been expressed in the form of a modal equation using the modal functions determined in (c). From the solution of the modal equation, responses of the liquid surface displacement and the slosh force and moment have been determined.

(e) When the Bond number is decreased, the dimensionless eigenfrequency decreases for high liquid-filling levels, but it increases for low liquid-filling levels.

(f) When surface tension is neglected, the analysis underestimates the magnitude of the liquid surface oscillation.

(g) The liquid-filling level which yields the maximum of slosh force and moment increases with decreasing Bond number.

ACKNOWLEDGMENTS

The author would like to thank the editor Dr M. P. Païdoussis and the referees for their useful comments. The author is grateful to Mr Dirk Riechelmann (Ishikawajima-Harima Heavy Industries Company, Ltd) for his correction of the manuscript.

TABLE 3
Convergence of numerical result for slosh force with increasing dimension of eigenvalue problem; all entries in the table are in percent (%)

(a) Bo = 1				(b) Bo = 10			
$\bar{k}$	$z_c = 0{\cdot}5$	$z_c = 1{\cdot}1$	$z_c = 1{\cdot}7$	$\bar{k}$	$z_c = 0{\cdot}5$	$z_c = 1{\cdot}1$	$z_c = 1{\cdot}7$
1	231·1	186·2	132·8	1	144·3	112·5	105·2
2	170·1	138·2	106·8	2	121·4	106·1	101·1
3	150·5	126·5	104·0	3	114·8	103·6	100·0
4	137·3	119·0	102·6	4	110·8	102·5	100·0
5	127·4	113·7	101·8	5	107·9	101·8	100·0
6	119·6	109·7	101·2	6	105·6	101·3	100·0
7	113·4	106·5	100·8	7	103·8	100·9	100·0
8	108·1	104·0	100·5	8	102·3	100·5	100·0
9	103·7	101·8	100·2	9	101·1	100·2	100·0
10	100·0	100·0	100·0	10	100·0	100·0	100·0
(c) Bo = 100				(d) Bo → ∞			
1	106·5	97·9	98·1	1	98·6	96·7	96·5
2	102·8	99·6	99·3	2	98·9	98·3	96·6
3	101·6	99·9	99·5	3	99·3	99·0	97·6
4	101·1	99·9	99·6	4	99·5	99·3	98·3
5	100·7	99·9	99·7	5	99·6	99·5	98·8
6	100·5	99·9	99·8	6	99·7	99·7	99·2
7	100·4	99·9	99·9	7	99·8	99·8	99·5
8	100·2	100·0	99·9	8	99·9	99·9	99·7
9	100·1	100·0	100·0	9	100·0	99·9	99·9
10	100·0	100·0	100·0	10	100·0	100·0	100·0

REFERENCES

ABRAMSON, H. N. (ed.) 1966 The dynamic behavior of liquids in moving containers, NASA Report SP-106.

BAUER, H. F. & SIEKMANN, J. 1971 Dynamic interaction of a liquid with the elastic structure of a circular cylindrical container, *Ingenieur-Archiv* **40,** 266–280.

CHU, W. H. 1970 Low-gravity fuel sloshing in an arbitrary axisymmetric rigid tank. *Journal of Applied Mechanics* **37,** 828–837.

CONCUS, P., CRANE, G. E. & SATTERLEE, H. M. 1969 Small amplitude lateral sloshing in spheroidal containers under low gravitational conditions. NASA Report CR-72500, LMSC-A944673, Lockheed Missiles and Space Company. Sunnyvale, California.

DODGE, F. T. & GARZA, L. R. 1967 Experimental and theoretical studies of liquid sloshing at simulated low gravity. *Journal of Applied Mechanics* **34,** 555–562.

DODGE, F. T. & GARZA, L. R. 1970 Simulated low-gravity sloshing in spherical, ellipsoidal, and cylindrical tanks. *Journal of Spacecraft and Rockets* **7,** 204–206.

DODGE, F. T., GREEN, S. T. & CRUSE, M. W. 1991 Analysis of small-amplitude low gravity sloshing in axisymmetric tanks. *Microgravity Science and Technology* **4,** 228–234.

HUNG, R. J. & LEE, C. C. 1992 Similarity rules in gravity jitter-related spacecraft liquid propellant slosh waves excitation. *Journal of Fluids and structures* **6,** 493–522.

NEU, J. T. & GOOD, R. J. 1963 Equilibrium behavior of fluids in containers at zero gravity. *AIAA Journal* **1,** 814–819.

PETERSON, L. D., CRAWLEY, E. F. & HANSMAN, R. J. 1989 Nonlinear fluid slosh coupled to the dynamics of a spacecraft. *AIAA Journal* **27,** 1230–1240.

SATTERLEE, H. M. & REYNOLDS, W. C. 1964 The dynamics of the free liquid surface in cylindrical containers under strong capillary and weak gravity conditions. Technical Report LG-2, Department of Mechanical Engineering, Stanford University, Stanford, CA., U.S.A.

SELIGER, R. L. & WHITHAM, G. B. 1968 Variational principles in continuum mechanics. *Proceedings of the Royal Society of London* A**305,** 1–25.

TONG, P. 1967 Liquid motion in a circular cylindrical container with a flexible bottom. *AIAA Journal* **5,** 1842–1848.

UTSUMI, M. 1988 Liquid sloshing in an axisymmetric container in low-gravity environments. In *Proceedings of the Sixteenth International Symposium on Space Technology and Science*. pp. 815–826.

UTSUMI, M. 1989 The meniscus and sloshing of a liquid in an axisymmetric container at low-gravity. In *Sloshing and Fluid Structure Vibration* (eds D. C. Ma, J. Tani, S. S. Chen & W. K. Liu), PVP-Vol. 157, pp. 103–113. New York: ASME.

YEH, C. K. 1967 Free and forced oscillations of a liquid in an axisymmetric tank at low-gravity environments. *Journal of Applied Mechanics* **34,** 23–28.

APPENDIX A: DERIVATION OF EQUATION (18)

Equation (18) can be proved by expressing $\mathrm{div}\,\mathbf{N}_F$ as the limit of a surface integral, i.e.

$$\mathrm{div}\,\mathbf{N}_F = \lim_{D\to 0}\left\{\oiint_A \mathbf{N}_F\cdot\mathbf{n}\,\mathrm{d}A/D\right\}, \tag{A1}$$

where D is an arbitrary volume including point P in which the vector $\mathbf{N}_F$ is erected, A is the closed surface bounding volume D, and $\mathbf{n}$ is the outer normal unit vector of surface A. Let volume D be the domain which the surface element $\mathrm{d}F$ penetrates during the virtual displacement $\delta\zeta$ from $\mathrm{d}F$ to $\mathrm{d}F' = \mathrm{d}F + \delta(\mathrm{d}F)$ (see Figure A1). Then, the inner product $\mathbf{N}_F\cdot\mathbf{n}$ is -1 on $\mathrm{d}F$, 1 on $\mathrm{d}F'$, and 0 on $A - \mathrm{d}F - \mathrm{d}F'$ (i.e. on all other portions of A, except $\mathrm{d}F$ and $\mathrm{d}F'$), while $D = \mathrm{d}F\ \delta\zeta\cos\gamma_F$. So, equation (A1) gives

$$\mathrm{div}\,\mathbf{N}_F = \frac{\mathrm{d}F' - \mathrm{d}F}{\mathrm{d}F\,\delta\zeta\cos\gamma_F} = \frac{\delta(\mathrm{d}F)}{\mathrm{d}F\,\delta\zeta\cos\gamma_F}, \tag{A2}$$

which is identical to equation (18).

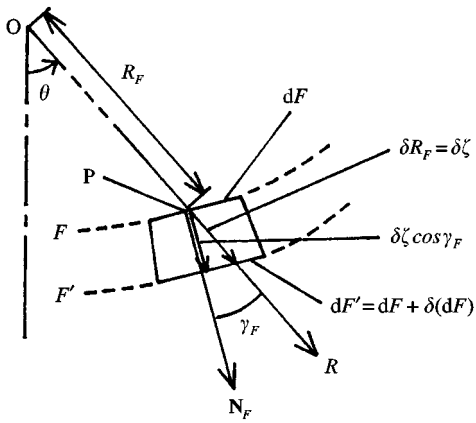

Figure A1. Virtual displacement of liquid surface F considered for derivation of equation (18).

APPENDIX B: DERIVATION OF EQUATION (53)

The new variables

$$\xi = \cos\theta, \qquad u(\xi) = (1 - \xi^2)^{-m/2}\Theta(\theta) \tag{B1}$$

transform equation (48) to a differential equation with regular singular points at $\xi = \pm 1$:

$$\frac{\mathrm{d}^2u}{\mathrm{d}\xi^2} - \frac{2(m+1)\xi}{1-\xi^2}\frac{\mathrm{d}u}{\mathrm{d}\xi} + \frac{\lambda - m(m+1)}{1-\xi^2}u = 0, \tag{B2}$$

which can be solved by a power-series expansion method. Substituting

$$u(\xi) = (\xi - 1)^\rho \sum_{i=0}^{\infty} a_i(\xi - 1)^i \tag{B3}$$

into equation (B2), one obtains an equation for ρ, namely

$$\rho(\rho + m) = 0, \tag{B4}$$

and a recurrence relation for the coefficients a_i:

$$a_{i+1} = \frac{\lambda - i(i+1) - m(m+1+2i)}{2(i+1)(i+1+m)}\, a_i\,. \tag{B5}$$

Equation (B4) yields $\rho = 0$, since the solution (B3) must be bounded at $\xi = 1$ ($\theta = 0$). The characteristic values $\lambda = \lambda_k$ ($k = 1, 2, \ldots$) must be determined such that the solution (B3) satisfies the boundary condition (50). By using equation (49) as well as equation (B1), the required system of characteristic functions $\Theta_k(\theta)$ can be expressed in terms of the Gauss hypergeometric series as equation (53).

APPENDIX C: DISCUSSION ON THE DYNAMIC CONTACT LINE CONDITION (EQUATION (57))

Calculating $\mathbf{N}_F \cdot \mathbf{N}_W$ from equations (25) and (26), expressing the result in the form of a Taylor expansion with respect to the liquid surface displacement and its derivatives, and considering only its linear component, we have

$$\Delta\cos\theta_c = -\sin\theta_c\,\Delta\theta_c = -\varepsilon[R_M(R_M\zeta_\theta - R_{M\theta}\zeta)/(R_M^2 + R_{M\theta}^2)^{3/2}\}_{\theta=\bar\theta}, \tag{C1}$$

where θ_c is the static contact angle, while $\Delta\theta_c$ denotes the time variation of the contact angle due to sloshing. The generatrix of the container wall is considered straight within a small range in which the contact line moves up and down during small amplitude sloshing. Since

$$\sin\theta_c = [R_M/(R_M^2 + R_{M\theta}^2)^{1/2}]_{\theta=\bar\theta}, \tag{C2}$$

we obtain from equation (C1)

$$\Delta\theta_c = \varepsilon[(R_M\zeta_\theta - R_{M\theta}\zeta)/(R_M^2 + R_{M\theta}^2)]_{\theta=\bar\theta}. \tag{C3}$$

Using approximation (57) and

$$(R_{M\theta}/R_M)_{\theta=\bar\theta} = -\varepsilon/\tan\theta_c\,, \tag{C4}$$

equation (C3) can be written as

$$\Delta\theta_c = -\varepsilon\,[R_{M\theta}\,\zeta/(R_M^2 + R_{M\theta}^2)]_{\theta=\bar\theta} = 0.5\sin(2\theta_c)(\zeta/R_M)_{\theta=\bar\theta}\,. \tag{C5}$$

Hence, the relative error is given by

$$\Delta\theta_c/\theta_c = (\zeta/R_M)_{\theta=\bar{\theta}} \tag{C6}$$

for a small static contact angle θ_c. For small amplitude sloshing in a spherical container, e.g. $\zeta_{\theta=\bar{\theta}} = 0{\cdot}1$ (10% of the container radius), the relative error is 10% for $z_c = 1{\cdot}71$ ($R_M = 1$, Figure 1). For z_c closer to 1, the error is smaller, and for $z_c = 1{\cdot}9$ it is still only 20%.

Looking into the derivation of equation (C5), we can find the reason why the relative error is restricted in spite of the very simple condition (57) and the small θ_c. For $\theta_c \to 0$ [i.e. $|R_{M\theta}| \to \infty$ from equation (C4)], the denominator of equation (C5), which contains the factor $R_{M\theta}^2$, becomes larger than the numerator which goes only with $R_{M\theta}$. This is nothing but the result of the special way of defining the spherical coordinate system (Figure 1). Figure 1 also gives us the following geometrically intuitive comprehension. There is only a little margin remaining for the rotation of the liquid surface ζ at the contact line, namely the small static contact angle θ_c, so that $\Delta\theta_c$ is controlled with the reduction of θ_c.

APPENDIX D: MATRIX COMPONENTS OF EQUATION (58)

The (k, l) components of the matrices in equation (58) are presented by

$$M_{ba}(k,l) = \varepsilon \int_0^{\bar{\theta}} \left[\left\{ f'_{al}\left(\frac{R_W}{l_a}\right)\frac{\Theta_l}{l_a} - \frac{R_{W\theta}}{R_W^2} f_{al}\left(\frac{R_W}{l_a}\right)\Theta'_l \right\} f_{bk}\left(\frac{R_W}{l_a}\right) R_w^2 \right.$$
$$\left. - \left\{ f'_{al}\left(\frac{R_M}{l_a}\right)\frac{\Theta_l}{l_a} - \frac{R_{M\theta}}{R_M^2} f_{al}\left(\frac{R_M}{l_a}\right)\Theta'_l \right\} f_{bk}\left(\frac{R_M}{l_a}\right) R_M^2 \right] \Theta_k \sin\theta \, \mathrm{d}\theta, \tag{D1}$$

$$M_{ac}(k,l) = \varepsilon \int_0^{\bar{\theta}} \Theta_l R_M^2 \sin\theta f_{ak}\left(\frac{R_M}{l_a}\right)\Theta_k \, \mathrm{d}\theta, \tag{D2}$$

$$M_{bc}(k,l) = \varepsilon \int_0^{\bar{\theta}} \Theta_l R_M^2 \sin\theta f_{bk}\left(\frac{R_M}{l_b}\right)\Theta_k \, \mathrm{d}\theta, \tag{D3}$$

$$M_{ca}(k,l) = -M_{ac}(l,k), \tag{D4}$$

$$M_{cb}(k,l) = -M_{bc}(l,k), \tag{D5}$$

$$K_{cc}(k,l) = \int_0^{\bar{\theta}} \left\{ \Theta_l \cos\theta + \frac{1}{\mathrm{Bo}}(S_{1M}\Theta_l + S_{2M}\Theta'_l + S_{3M}\Theta''_l - m^2 S_{4M}\Theta_l) \right\} R_M^2 \sin\theta \Theta_k \, \mathrm{d}\theta, \tag{D6}$$

where

$$f_{ak}(x) = x^{\alpha_1 k}, \qquad f_{bk}(x) = x^{\alpha_2 k}. \tag{D7}$$

The matrix components which are not listed can be determined as follows: $M_{aa}(k,l)$ is determined by replacing suffix b in equation (D1) by a, $M_{bb}(k,l)$ is determined by replacing suffix a in equation (D1) by b and $M_{ab}(k,l) = M_{ba}(l,k)$.

APPENDIX E: COEFFICIENTS IN MODAL EQUATION (67)

The coefficients in equation (67) are presented by

$$M = \sum_{k=1}^{\infty}\sum_{l=1}^{\infty} \int_0^{\bar{\theta}} [a_k a_l \bar{M}_{aa}(k,l) + a_k b_l \{\bar{M}_{ab}(k,l) + \bar{M}_{ba}(l,k)\} + b_k b_l \bar{M}_{bb}(k,l)$$

$$+ a_k c_l \{\bar{M}_{ac}(k,l) + \bar{M}_{ca}(l,k)\} + b_k c_l \{\bar{M}_{bc}(k,l) + \bar{M}_{cb}(l,k)\}] \, \mathrm{d}\theta, \tag{E1}$$

$$K = \sum_{k=1}^{\infty} \sum_{l=1}^{\infty} \int_0^{\bar{\theta}} c_k c_l \bar{K}_{cc}(k,l) \, \mathrm{d}\theta, \tag{E2}$$

$$\beta = -\varepsilon \sum_{k=1}^{\infty} c_k \int_0^{\bar{\theta}} R_M^3 \sin^2\theta \Theta_k \, \mathrm{d}\theta. \tag{E3}$$

In equations (E1) and (E2), $\bar{M}_{aa}(k,l)$, etc. are given by

$$\bar{M}_{\alpha\beta}(k,l) = \varepsilon f_{\alpha k}(R_W/l_\alpha)\Theta_k \sin\theta \{R_W^2 f'_{\beta l}(R_W/l_\beta)\Theta_l/l_\beta - R_{W\theta} f_{\beta l}(R_W/l_\beta)\Theta'_l\}$$
$$- \varepsilon f_{\alpha k}(R_M/l_\alpha)\Theta_k \sin\theta \{R_M^2 f'_{\beta l}(R_M/l_\beta)\Theta_l/l_\beta - R_{M\theta} f_{\beta l}(R_M/l_\beta)\Theta'_l\},$$

in which $(\alpha, \beta) = (a, a), (a, b), (b, a), (b, b)$;

$$\begin{aligned}
\bar{M}_{ac}(k,l) &= \varepsilon R_M^2 \sin\theta f_{ak}(R_M/l_a)\Theta_k\Theta_l, \\
\bar{M}_{bc}(k,l) &= \varepsilon R_M^2 \sin\theta f_{bk}(R_M/l_b)\Theta_k\Theta_l, \\
\bar{M}_{ca}(k,l) &= \bar{M}_{ac}(l,k), \; \bar{M}_{cb}(k,l) = \bar{M}_{bc}(l,k), \\
\bar{K}_{cc}(k,l) &= -R_M^2 \sin\theta\Theta_k\{\Theta_l \cos\theta + (S_{1M}\Theta_l + S_{2M}\Theta'_l + S_{3M}\Theta''_l - m^2 S_{4M}\Theta_l)/\mathrm{Bo}\},
\end{aligned} \tag{E4}$$

where both α and β may stand for a or b in the first equation.

APPENDIX F: NOMENCLATURE

a_k, b_k	coefficients in modal function for velocity potential
Bo	Bond number
b	half-height of container (characteristic length, Figure 1)
c_k	coefficients in modal function for liquid surface displacement
$\mathbf{e}_R$, $\mathbf{e}_\theta$, $\mathbf{e}_\varphi$	unit vectors in R, θ and φ directions
F	disturbed liquid surface (Figure 1)
F_x	slosh force
$\ddot{f}(t)$	lateral acceleration of container
$G(t)$	arbitrary function in pressure equation (12)
g	gravitational acceleration
$\mathbf{i}$, $\mathbf{j}$, $\mathbf{k}$	unit vectors in x, y and z- directions
$\bar{k}$	number of characteristic functions Θ_k taken into account
l_a, l_b	normalization parameters [equation (55)]
M	meniscus (undisturbed liquid surface, Figure 1)
M_y	slosh moment
m	circumferential wave number
$\mathbf{N}_F$	unit normal vector of F pointing into liquid domain
$\mathbf{N}_W$	unit normal vector of W pointing outwards from liquid domain
p_0	static liquid pressure at bottom ($r = 0$) of meniscus
p_c	static liquid pressure at contact line
p_g	gas pressure
p_l	liquid pressure
$q(t)$	modal coordinate
R, θ, φ	spherical coordinates (Figure 1)
$R_F(0, \varphi, t)$	function expressing shape of disturbed liquid surface (Figure 1)

$R_M(\theta)$	function expressing shape of undisturbed liquid surface (Figure 1)
$R_W(\theta)$	function expressing shape of container wall (Figure 1)
$S_{0M} - S_{4M}$	θ-dependent functions [equation (33)]
V	liquid domain (Figure 1)
W	container wall (Figure 1)
z_c	z-coordinate of the contact line
z_0	z-coordinate of meniscus bottom ($r = 0$)
α_{1k}, α_{2k}	characteristic exponents [equations (54) and (55)]
γ_F	angle between $\mathbf{N}_F$ and R-direction
ε	1 and -1, respectively, for Cases 1 and 2 (Figure 1)
ζ	liquid surface displacement (Figure 1)
$\boldsymbol{\Theta}_k$	characteristic function determined by equations (48) and (50)
$\bar{\theta}$	maximum of θ (Figure 1)
θ_c	contact angle between meniscus and container wall
λ_k	characteristic value determined by equations (48) and (50)
ρ_f	liquid density
σ	surface tension (surface free energy per unit area)
$\boldsymbol{\Phi}$	velocity potential
ϕ	velocity potential (relative motion to container)
ω_g	characteristic frequency [equation (40)]

Subscripts

k	characteristic value and function number
θ	differentiation with respect to θ
φ	differentiation with respect to φ